Remote Spectral Measurement Using Entangled Photons

Giuliano Scarcelli, Alejandra Valencia, Samuel Gompers and Yanhua Shih

Department of Physics, University of Maryland, Baltimore County, Baltimore, Maryland 21250

Abstract

By utilizing the frequency anticorrelation of two-photon states produced via spontaneous parametric down conversion (SPDC), the working principle of a novel remote spectrometer is demonstrated. With the help of a local scanning monochromator, the spectral transmission function of an optical element (or atmosphere) at remote locations can be characterized for wide range of wavelengths with expected high resolution.

1

Two-photon states generated via SPDC have been a very resourceful tool for studying fundamental aspects of quantum theory [1]. Recently also their practical applications have been exploited opening new fields like quantum information processing, quantum metrology, quantum imaging and quantum lithography [2]. In this paper we use SPDC as a frequency anticorrelated two-photon source to demonstrate the working principle of a novel remote spectrometer: a local scanning monochromator is located in a laboratory, but it defines the wavelength measured at remote locations because of the frequency anticorrelation between photons in a pair emitted by SPDC. The process is equivalent to carry a "conjugate monochromator" to remote locations. The proposed method shows a number of interesting features: SPDC sources offer the natural possibility of wide spectral ranges of operation, and due to the frequency anticorrelation between the two photons in a pair and the coincidence-like type of detection, it is possible to make the two detectors operate in very different spectral regions without affecting the measurement with spurious signals and without changing the resolution of the measurement determined by the local monochromator.

The process of SPDC involves passing a pump laser beam through a nonlinear material, for example, a non-centrosymmetric crystal. Occasionally, the coherent nonlinear interaction leads to the annihilation of a high frequency pump photon and the simultaneous creation of two lower frequency photons, signal and idler, which satisfy the phase matching conditions [3]:

$$\omega_p = \omega_s + \omega_i, \quad \mathbf{k}_p = \mathbf{k}_s + \mathbf{k}_i \tag{1}$$

where ω_j, $\mathbf{k}_j$ (j = s, i, p) are frequencies and wavevectors of the signal (s), idler (i), and pump (p) respectively.

The schematic setup of the remote spectrometer is shown in Fig. 1. Photon pairs are generated through the SPDC process in a local laboratory. The signal photon is sent to a remote location (e.g. space) passing through the optical element (or atmosphere) whose transmission spectral function is to be measured. The idler photon passes through a monochromator in the laboratory. The signal and the idler are then detected by photon counting detectors

D_1, in the space, and D_2, in the laboratory. Each detector is connected to an event timer, an electronic device that records the registration time history at which a "click" detection event on the detector has occurred [4]. The registration time history of detector D_1 of the space station is sent back to the laboratory through a classical communication channel (telephone, internet etc.). The two individual registration time-histories are analyzed to achieve maximum "coincidences" by shifting the time bases of the two. The remote spectrometer is now properly set. The spectral function of the remote spectral filter is obtained by measuring the rate of coincidence counts at each wavelength defined by the monochromator.

Perhaps the most important feature of the remote spectrometer is the enormous range of wavelengths that can be analyzed. This aspect comes, as previously mentioned, from the frequency correlation between the signal and idler photons. According to Eq. (1), if a pump laser at $400nm$ is used, a scanning monochromator working in the visible region ($400nm - 700nm$) will be able to remotely analyze a virtually infinitely large range of infrared wavelengths. The resolution of the remote characterization will be determined by the monochromator's inherent resolution. Thus, using a high resolution monochromator in visible wavelengths will permit high resolution calibrations in infrared wavelengths.

Considering the experimental setup in Fig. 1, the joint detection counting rate, R_c, of detectors D_1 and D_2, on the time interval T, is given by the Glauber formula [5]:

$$R_c \propto \frac{1}{T} \int_0^T \int_0^T dt_1 dt_2 \, G^{(2)}(t_1, r_1; t_2, r_2) \tag{2}$$

In Eq. (2) $G^{(2)}(t_1, r_1; t_2, r_2)$ is the second order correlation function defined as:

$$G^{(2)}(t_1, r_1; t_2, r_2) \equiv |\langle 0| E_2^{(+)}(t_2, r_2) E_1^{(+)}(t_1, r_1) |\Psi\rangle|^2 = |\psi(t_1, r_1; t_2, r_2)|^2 \tag{3}$$

Here ψ is defined as the effective two-photon wavefunction [6]. $E_i^{(\pm)}(t_i, r_i)$, $i = 1, 2$, are positive-frequency and negative-frequency components of the field at detectors D_1 and D_2 that can be written as:

$$E_1^{(+)}(t_1, r_1) = \int d\omega \, f(\omega) \, a(\omega) \, e^{-i[\omega t_1 - k(\omega) r_1]}$$
$$E_2^{(+)}(t_2, r_2) = \int d\omega \, \Pi(\omega - \omega_M) \, a(\omega) \, e^{-i[\omega t_2 - k(\omega) r_2]} \tag{4}$$

3

where $f(\omega)$ is the spectral function to be measured and $\Pi(\omega - \omega_M)$ simulates the spectral function of the monochromator: a narrow-bandpass function centered at wavelength ω_M.

The signal-idler two-photon state of SPDC can be calculated by applying the first order perturbation theory of quantum mechanics [3]. Restricting the calculation to one dimension and collinear SPDC, the two-photon state is:

$$|\Psi\rangle = \int_{-\infty}^{\infty} d\nu \, \Phi(\nu) \, a_s^\dagger(\omega_s^0 + \nu) \, a_i^\dagger(\omega_i^0 - \nu) \, |0\rangle \,, \tag{5}$$

where $\Phi(\nu)$ is the spectral amplitude of SPDC and is determined by the wavevector phase matching inside the nonlinear crystal, $a^\dagger$ is the photon creation operator, $|0\rangle$ denotes the vacuum state. Here ω_s^0 and ω_i^0 are the central frequencies of the signal-idler radiation field, ν is a parameter satisfying:

$$\omega_s = \omega_s^0 + \nu, \quad \omega_i = \omega_i^0 - \nu, \quad \omega_s^0 + \omega_i^0 = \omega_p, \tag{6}$$

Using Eq. (4) and Eq. (5), and expanding the wavevector k to the second order in ν, the effective two-photon wave function becomes:

$$\psi(\tau) = \int d\nu \, \Phi(\nu) \, f(\omega_s^0 + \nu)\Pi(\omega_i^0 - \nu - \omega_M e^{-i\nu\tau} e^{-\frac{i[k_1'' r_1 + k_2'' r_2]\nu^2}{2}} \tag{7}$$

where $\tau \equiv [(t_2 - \frac{r_2}{u_2}) - (t_1 - \frac{r_1}{u_1})]$; $u_{1,2} \equiv 1/k_{1,2}'(\omega_{s,i}^0)$ are the inverse first order dispersions of the media in which the signal and the idler propagate. Eq. (7) indicates that $\psi(\tau)$ is the Fourier transform of a product of four functions. The second order dispersion of the media will contribute to the broadening of the function $G^{(2)}$ [7]: depending on the propagation distance, this broadening may affect the operational decision of the "coincidence" time window width. The second order dispersion can be "cancelled" by introducing into the optical path a different type of dispersive material that has the same magnitude of second order dispersion but an opposite sign [8], see Eq. (7). Based on these considerations, we will ignore the second order dispersion in the following. In this case, we can treat $\Pi(\omega_i^0 - \nu - \omega_M)$ as a δ-function if $f(\omega_s^0 + \nu)$ and $\Phi(\nu)$ are much wider then $\Pi(\omega_i^0 - \nu - \omega_M)$. $G^{(2)}(\tau)$ becomes:

$$G^{(2)} \sim |\int d\nu \, \Phi(\nu) \, f(\omega_s^0 + \nu)\delta(\omega_i^0 - \nu - \omega_M) \, e^{-i\nu\tau} |^2 \tag{8}$$

4

and the coincidence counting rate is then:

$$R_c \sim |\Phi(\omega_i^0 - \omega_M)\, f(\omega_p - \omega_M)|^2 \qquad (9)$$

Furthermore, if $\Phi(\omega_i^0 - \omega_M)$ is relatively flat compared to function $f(\omega_p - \omega_M)$, which can be achieved experimentally, Eq. (9) becomes,

$$R_c \sim |f(\omega_p - \omega_M)|^2 \qquad (10)$$

i.e the rate of coincidence counts reproduces exactly the spectral function of the remote optical element, but reversed in frequency with respect to the frequency of the pump.

The detailed experimental demonstration setup is shown in the lower part of Fig. 1. An Argon ion laser line of $457.9nm$ was used to pump a 8mm LBO crystal for SPDC. The LBO was cut for type II degenerate collinear phase matching. The LBO crystal was slightly tilted in the case of non-degenerate collinear phase matching. After passing through the crystal, the pump beam was blocked by two mirrors with high reflectivity at the pump wavelength and by a Newport RG715 color glass filter. The orthogonally polarized photon pair was then split by a polarizing beam splitter. The transmitted signal photons were detected by a single-photon counting module D_1 (Perkin-Elmer SPCM-AQR-14) after passing through the optical element to be characterized. The reflected idler photons were sent to a monochromator (CVI Digikrom CM110) with $2nm$ resolution through a $38mm$ focal length lens. A $50mm$ focal length lens was placed at its focal distance from the LBO crystal in order to collect the necessary wide spectrum of SPDC radiation into the monochromator. The output of the monochromator was then collected and detected by another single-photon counting module D_2. The photocurrent pulses from detectors D_1 and D_2 were then sent to the "coincidence counting circuit" with $5ns$ integrating time window.

In order to meet the requirement that led to Eq. (10), in which we assumed a relatively flat SPDC spectrum, $\Phi(\omega_i^0 - \omega_M)$, compared to the filter function, $f(\omega_p - \omega_M)$, we needed to collect the entire region of relevant SPDC spectrum and couple all the wavelengths into the monochromator with the same efficiency. The choice of the lenses was made exactly to pursue this objective.

Fig. 2, Fig. 3 and Fig. 4 report three typical measurements for bandpass filters centered at $850nm$, $885.6nm$ and $916nm$ with bandwidths of $10nm$, $11nm$ and $10nm$, respectively. In the graphs, we provided two scales of wavelengths, referred to the signal and the idler wavelengths. These wavelengths can also be read as local "actually" measured wavelength (λ-idler) and "remote" indirectly measured wavelength (λ-signal). The reported single detector counting rates of D_2 are slightly "tilted" at longer wavelengths. The tilting slope is mainly determined by the coupling efficiency of the monochromator [9]. To account for this, we normalized the coincidence counts accordingly (see figure captions for details). It is clear from these experimental data that the remote measurements agree with the standard laboratory classical spectral transmissivity calibration curves and with the theoretical predictions.

REFERENCES

[1] A.Einstein, B.Podolsky, N.Rosen, Phys. Rev. **47**, 777 (1935).

[2] See for example recent review papers: J.P. Dowling, G.J. Milburn, quant-ph/0206091 and A. Migdall, Physics Today **52**, 41 (1999).

[3] D.N. Klyshko, *Photons and Nonlinear Optics* (Gordon & Breach, New York,1988); A. Yariv, *Quantum Electronics*, John Wiley and Sons, New York, (1989).

[4] C. Steggerda *et al*, Proceedings of the 10th International Workshop on Laser Ranging Instrumentation, Ed. F.M. Yang, Chinese Academy of Sciences Press, 404 (1996).

[5] R.J. Glauber, Phys. Rev. **130**, 2529 (1963); **131**, 2766 (1963).

[6] M.H. Rubin, D.N. Klyshko, Y.H. Shih, and A.V. Sergienko, Phys. Rev. A **50**, 5122 (1994).

[7] A.Valencia, M.V.Chekhova, A.Trifonov and Y.Shih, Phys. Rev. Lett. **88**, 183601 (2002).

[8] J.D. Franson, Phys. Rev. A, **45**, 3126 (1992).

[9] W.Demtroder, *Laser Spectroscopy* (2nd edition, Springer, 1998).

FIGURES

FIG. 1. Scheme of a remote spectrometer and the experimental setup

FIG. 2. Experimental characterization of a $10nm$ bandpass filter centered at $850nm$. The solid line is a direct measurement of the transmissivity function of the $850nm$ spectral filter by using classical method; hollow squares are the single counts of detector D_1 ($\sim$ 2.5 Mc/second); filled squares are the single counts of detector D_2 (peak of $\sim$ 10 Kc/s). The circles are the normalized coincidence counts weighted by the single counts of detector D_2 (peak of $\sim$ 900 cc/s).

FIG. 3. Experimental characterization of a $11nm$ bandpass filter centered at $885.6nm$. The solid line is the standard characterization; hollow squares are the single counts of D_1 ($\sim$ 3 Mc/s); filled squares are the single counts of D_2 (peak of $\sim$ 12 Kc/s). The circles are the normalized cc weighted by the single counts of D_2 (peak of $\sim$ 1100 cc/s) .

FIG. 4. Experimental characterization of a $11nm$ bandpass filter centered at $916nm$. The solid line is the standard characterization; hollow squares are the single counts of D_1 ($\sim$ 1.5 Mc/s); filled squares are the single counts of D_2 (peak of $\sim$ 10 Kc/s). The circles are the normalized cc weighted by the single counts of D_2 (peak of $\sim$ 900 cc/s).
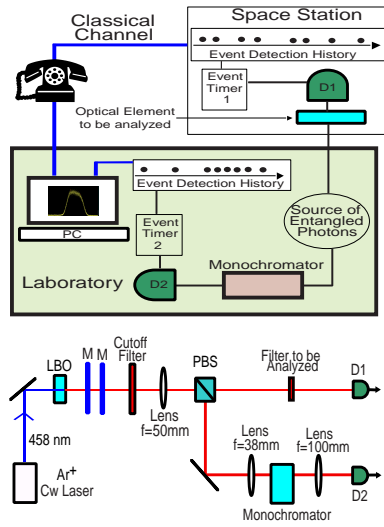
Figure 1. Giuliano Scarcelli, Alejandra Valencia, Samuel Gompers , and Yanhua Shih.
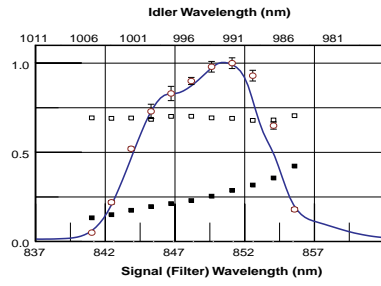
Figure 2. Giuliano Scarcelli, Alejandra Valencia, Samuel Gompers , and Yanhua Shih.
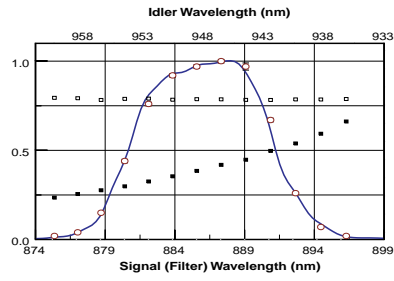
Figure 3. Giuliano Scarcelli, Alejandra Valencia, Samuel Gompers , and Yanhua Shih.
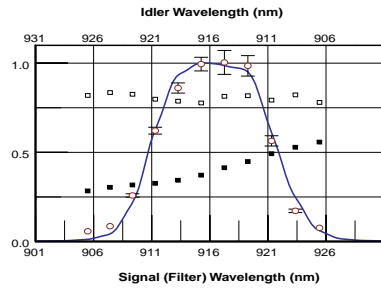
Figure 4. Giuliano Scarcelli, Alejandra Valencia, Samuel Gompers , and Yanhua Shih.